Optics & Laser Technology 43 (2011) 996–1005

Contents lists available at ScienceDirect

Optics & Laser Technology

journal homepage: www.elsevier.com/locate/optlastec

Using the camera pin-hole model restrictions to calibrate the lens distortion model

Carlos Ricolfe-Viala *, Antonio-José Sánchez-Salmerón

Universidad Politecnica de Valencia, Engineering Systems and Automatic Control Department, Camino de Vera s/n, 46022 Valencia, Spain

ARTICLE INFO

Article history:
Received 7 September 2010
Accepted 5 January 2011
Available online 3 February 2011

Keywords:
Camera calibration
Lens distortion
Distortion model

ABSTRACT

Camera calibration required the computation of camera pin-hole and lens distortion models. The lens distortion is estimated alone or together with the pin-hole model, by using some existing lens distortion non-metric or self-calibration methods. If both models are computed together, then the models are adjusted to training data, but not to real camera. This is because both pin-hole and lens distortion models are coupled. If they are computed separately, difficulties arise since calibration of lens distortion alone is an unstable process. To improve existing camera calibration methods, this paper proposes a metric calibration method to compute lens distortion separately from the pin-hole model. This method is solved under stable conditions, independently of the computed lens distortion model, since pin-hole and distortion models are computed separately. Images of a planar template are used. First, using distorted control points extracted from images, a set of undistorted points which fits in the pin-hole model are computed. Second, with distorted and undistorted control points, lens distortion is calibrated by using a metric calibration process.

1. Introduction

Camera calibration is required to obtain pin-hole camera lens distortion models. The pin-hole model is composed with intrinsic and extrinsic parameters. Intrinsic parameters contain the geometry of the camera and the optical features of the sensor. Extrinsic parameters map the 3D points in the scene to the coordinate system of the camera. The pin-hole model simplifies many of the geometric considerations involved and assumes ideal camera performance, which is seldom the case. Imperfections arise if low-cost video optics are used, especially wide-angle or fish-eye lenses, or in applications where a high degree of accuracy is required. When lens distortion is not negligible, a distortion-free model may result in a high calibration error [1]. In such cases, the pin-hole model is not sufficient and further parameters should be estimated to take lens distortion into account.

From the point of view of the distortion model, several models exist depending on the type of lens. Brown [2,3] proposed the radial, decentering and prism distortion model which has been modified in different forms [4–10]. If fish-eye or high distortion lenses are used higher order terms of radial, decentering and prism model are not able to represent this effect in the image. To resolve this problem, Basu and Licardie [4], Devernay and Faugeras [11], Fitzgibbon [12] and some others have defined general purpose distortion models and specific models for fish-eye lens distortion.

To identify each distortion model, several methods have been proposed. Some of them are called non-metric calibration or self-calibration methods and compute the distortion model without any information of the scene neither any calibration objects nor known structure. Self-calibration methods use geometric invariants of some image features like straight lines [3,11,13–15], vanishing points [16,17] or the image of a sphere [18]. Other methods rely on the fact that straight lines in the scene project on straight lines in the image [3,11,13–15]. In [16,17] the minimum vanishing point dispersion constraint between three mutually orthogonal sets of parallel lines is used to recover the distortion parameters. The problem with these methods is to find triple sets of orthogonal lines and obtain stable results in a general framework. Other methods use correspondences between points in different images from multiple views to compute camera distortion parameters [19,20,12]. In this case, these methods are not easy to solve and are likely to produce some false data in the distortion algorithm.

From the point of view of the pin-hole model calibration, a variety of methods have been developed for various applications [3,21–27] (among others). One family of pin-hole calibration methods resolves the camera model using metric information from a 3D, 2D and 1D template. The other family does not use any metric information from the scene and are known as the self-calibration methods. Self-calibration tends to be unstable if

* Corresponding author. Tel.: +34 963 877 007x88231; fax: +34 96 387 98 16.
E-mail addresses: cricolfe@isa.upv.es (C. Ricolfe-Viala), asanchez@isa.upv.es (A.-J. Sánchez-Salmerón).
URL: http://robotica.isa.upv.es/ (C. Ricolfe-Viala).

0030-3992/$ - see front matter © 2011 Elsevier Ltd. All rights reserved.
doi:10.1016/j.optlastec.2011.01.006

all camera parameters are unknown [1]. In these cases, known camera motion helps in getting more stable and accurate results [20,28], but "pure camera rotation" is not always easy to obtain. Better results are always achieved with metric calibration methods. Regarding the computed camera models, some only compute the pin-hole parameters [25], and others solve the pin-hole model together with the distortion parameters [21,22,24]. Since distortion is most often coupled with the internal and external camera parameters, methods which extend the calibration of the pin-hole model to obtain lens distortion parameters result in large errors in the internal parameters [22]. Thus, a method allowing a good accuracy for pin-hole and lens distortion calibration under stable conditions is not yet available. It is thus necessary to use a method which estimates the pin-hole and lens distortion models separately. Furthermore, if lens distortion is already known, control points can be corrected to obtain an accurate pin-hole calibration.

In this paper we propose a metric method for lens distortion and pin-hole model calibration. Here, the camera calibration process is understood as a two-step procedure. First, a set of points which fits in a camera pin-hole model and satisfy scene geometric restrictions is computed. Second, lens distortion model is calibrated using detected (thus distorted) control points in the image and the corrected undistorted control points computed together with the pin-hole model previously. With this calibration method, lens distortion and pin-hole models can be fully defined without risk of instabilities. The proposed method is based on the idea that the image of a structure maintains its proportions according to a perspective projection. Therefore, there are different magnitudes within the scene that are fixed independently of the position, orientation and characteristics of the camera that takes the image. This paper proposes a method for correcting the detected points in the image to fulfill restrictions given by the features of the calibration template and the pin-hole model, and to calibrate the lens distortion using both sets of points: the distorted detected in the image and the undistorted points which fits the pin-hole model.

The paper is organized as follows. Section 2 describes the camera lens distortion model. Section 3 proposes the basis of the metric calibration method: the geometric invariants of a structure independent of perspective projection and how the location of the set of points in the image is corrected according with the pin-hole model. Section 4 derives the calibration of the camera lens distortion model using both sets of points. Several experimental results are reported on both real and synthetic data and are also compared with non-metric camera lens distortion calibration methods. The paper ends with some concluding remarks.

2. Correcting fish-eye lens distortion

When fish-eye or other high-distortion lenses are used, a distortion model to obtain a wide-angle image of the scene is necessary. In these cases, higher order terms of radial, tangential and prism distortion model has been considered [9,29], although it does not fully satisfy the camera lens distortion [11]. Nevertheless, since higher order terms of radial, tangential and prism distortion components are not able to represent this effect in the image, it is better to use a distortion model that tries to mimic this effect. Following this idea, alternative distortion models have been developed to deal with fish-eye cameras, including the logarithmic or fish-eye transform [4], the polynomial fish-eye transform [4], the field of view model [11], and the division model [12,30]. On the validation and comparison of fish-eye lens models, Schneider et al. [31] and Hughes et al. [32] examine the accuracy of the various fish-eye projection functions using spatial resection and bundle adjustment. Evaluations conclude that precision of polynomial fish-eye transform model is larger than fish-eye or field of view models.

Basu and Licardie [4] based the polynomial fish-eye transformation model on the observation that fish-eyes have high resolution at the fovea, and non-linear decreasing towards the periphery. Let (r_p,α) denote the polar coordinates of a point $\boldsymbol{q_p}=(u_p,v_p)$ in the image, where $r_p^2=\Delta u_p^2+\Delta v_p^2$ and $\alpha=arctan(\Delta v_p/\Delta u_p)$, the distorted polar coordinates (r_d,α_d) can be obtained as

$$r_d = G(r_p) = a_0 + a_1 r_p + a_2 r_p^2 + \cdots a_n r_p^n = \sum_{i=0}^{k} a_i r_p^i, \quad \alpha_d = \alpha \tag{1}$$

where k represents the degree of the polynomial fish-eye distortion model. Basu and Licardie [4] found that fourth or fifth order for polynomial fish-eye transformation model is a reasonably good approximation of the average distortion. The corresponding distorted Cartesian coordinates $\boldsymbol{q_d}=(u_d, v_d)$ are given by

$$u_d = r_d \cos\alpha_d, \quad v_d = r_d \sin\alpha_d \tag{2}$$

Polynomial fish-eye distortion model can be calibrated following the method described in [4]. However, this method obtains a measure of distortion in the four different directions which can be unstable if few points are used.

3. Undistorting images and calibrating the pin-hole model

To find the undistortion that maps the actual camera image plane onto an image following the perspective camera pin-hole model, a two step method is proposed ($^{i,j}\boldsymbol{q}$ represent the image coordinate of a point in the scene $^{i}\boldsymbol{p}$ in the image j):

1. Calibrate the pin-hole model of the camera using detected control points in the image $^{i,j}\boldsymbol{q_d}$, and obtain the true points positions $^{i,j}\boldsymbol{q_p}$ of distorted points $^{i,j}\boldsymbol{q_d}$ in the image. $^{i,j}\boldsymbol{q_d}$ represents location of control point i in distorted image j and $^{i,j}\boldsymbol{q_p}$ represents its true position. The true position is computed using all constraints which are true with the control points in the calibration template and remain with the perspective projection. Control points correction and pin-hole model calibration is done together.
2. Adjust the distortion model using distorted control points $^{i,j}\boldsymbol{q_d}$ detected in the image and undistorted ones $^{i,j}\boldsymbol{q_p}$ computed in the previous step.

Steps 1 and 2 are defined in Sections 3.1 and 3.2, respectively.

3.1. Undistorting the set of points and computing the pin-hole model

The pin-hole model is defined as follows:

$$^{i,j}\boldsymbol{q} = A[R_j,t_j]^i p \tag{3}$$

Here, $^{i,j}\boldsymbol{q}$ is the image coordinates of the point $^{i}\boldsymbol{p}$ in the image j. $\boldsymbol{A}$ represents the intrinsic parameters matrix, $\boldsymbol{R}_j$ and $\boldsymbol{t}_j$ are the rotation matrix for image j, respectively. Depending on where control points are located in the scene, a three, two or one dimensional techniques can be used to calibrate the pin-hole model. If a three dimensional template is used, techniques described in [21–23], can be utilized. With two and one dimensional templates, techniques presented by Zhang [24,25] can be used. Revising the state of the art of camera calibration techniques, [33] demonstrates that the planar calibration approach exemplified by Zhang's method [24], makes efficient use of template information and requires neither a laborious measuring task nor specialized equipment. We have chosen the calibration technique based on a planar template to resolve the camera parameters and correcting points in the image.

Following [24], the two-dimensional calibration method can be summarized in a linear and a non-linear step. First, the linear step gives an approximation of camera's intrinsic and extrinsic parameters, which is refined using a non-linear searching. The non-linear step can include the intrinsic and extrinsic camera parameters only, or both the pin-hole and the lens distortion models. The non-linear step is solved with expression (10) of [24]:

$$J_{PH} = \sum_{j=1}^{m}\sum_{i=1}^{n}\left({}^{i,j}\boldsymbol{q} - g(\boldsymbol{A},\boldsymbol{R}_j,\boldsymbol{t}_j,{}^{i}\boldsymbol{p})\right)^2 \tag{4}$$

Here, m represents the number of images and n the number of points per image. In our proposed method, this non-linear searching is redefined, to obtain the camera pin-hole model, and the set of points which accomplishes the geometric invariants defined previously. We start with computing the approximation of the pin-hole model using the set of distorted control points extracted from the images ${}^{i,j}\boldsymbol{q_d}$ and the closed form solution described in Section 3.1 of [24]. Distortion is not computed now. To minimize function (4) the pin-hole model parameters and the distorted control points ${}^{i,j}\boldsymbol{q_d}$ are treated as variables. This means that the pin-hole model and control points are arranged together in a non-linear searching. $\boldsymbol{A}$, $\boldsymbol{R}_j$ and $\boldsymbol{t}_j$ searching starts with the approximated values computed in the linear step $\boldsymbol{A_c}$, $\boldsymbol{R_{cj}}$, $\boldsymbol{t_{cj}}$ and the search ends with the improved ones $\boldsymbol{A_p}$, $\boldsymbol{R_{pj}}$ and $\boldsymbol{t_{pj}}$. ${}^{i,j}\boldsymbol{q}$ searching starts with the distorted coordinated from the image ${}^{i,j}\boldsymbol{q_d}$, and it ends with corrected undistorted control points ${}^{i,j}\boldsymbol{q_p}$. ${}^{i}\boldsymbol{p}$ are fixed points' locations in the template. Fig. 1b,d,f shows distorted points ${}^{i,j}\boldsymbol{q_d}$ detected in the image and the computed corrected ones ${}^{i,j}\boldsymbol{q_p}$.

Analyzing Eq. (4), if pin-hole parameters and distorted points are treated as unknowns, we have an under constrained optimization problem. We have $2nm+5+6m$ unknowns from ${}^{i,j}\boldsymbol{q_d}$, $\boldsymbol{A}$, $\boldsymbol{R}_j$ and $\boldsymbol{t}_j$ and only $2nm$ residuals. Inspired in [34], restrictions which remain under perspective projection are imposed to minimize (4). Since we are using a chessboard pattern to resolve the calibration process, control points are arranged in a regular structured scene which remains in images of the scene. Points are arranged in straight lines which are parallel and perpendicular each other and also equidistant. If equidistant parallel and perpendicular straight lines are projected in an image restriction remains. Therefore, the cross-ratio, which is a ratio of ratios of distances, will be preserved under projective geometry and, straight lines will be always straight [11,15]. These two restrictions are going to be added to the optimization process.

If $\mathrm{CR}(\boldsymbol{p_1},\boldsymbol{p_2},\boldsymbol{p_3},\boldsymbol{p_4})$ represents the cross-ratio of four points in the template, it will be equal to all four set of points in the planar template which are equally distributed and in consequence, its corresponding points in the image. Distorted coordinates ${}^{i,j}\boldsymbol{q_d}$ must satisfy the cross-ratio $\mathrm{CR}(\boldsymbol{p_1},\boldsymbol{p_2},\boldsymbol{p_3},\boldsymbol{p_4})$ if they are corrected to its right positions ${}^{i,j}\boldsymbol{q_p}$. Points in the template are separated in r sets of s points which form straight lines, where r is the number of straight lines in the calibration template and s is the number of points in each line. $\boldsymbol{q}^{k,l}$ is a point k of the straight line l in one image, $l=1,\ldots,a$, $k=1,\ldots,b$. The following equation measures how a set of points are equally separated under perspective projection:

$$J_{CR} = \sum_{l=1}^{r}\sum_{k=1}^{s-3}\left(CR(q^k,q^{k+1,l},q^{k+2,l},q^{k+3,l}) - CR(\boldsymbol{p_1},\boldsymbol{p_2},\boldsymbol{p_3},\boldsymbol{p_4})\right)^2 \tag{5}$$

Taking into account that chessboard has straight lines in vertical and horizontal directions; this equation must be true for horizontal and vertical straight lines. Each point in the image ${}^{i,j}\boldsymbol{q_d}$ belongs to two lines and it represents the intersection. Thus, the cross-ratio of the point ${}^{i,j}\boldsymbol{q_d}$ with all its neighborhoods must be true in both directions. $\mathrm{CR}(\boldsymbol{p_1},\boldsymbol{p_2},\boldsymbol{p_3},\boldsymbol{p_4})$ is computed previously when the planar template is designed.

On the other hand, since points in the image have been separated in r straight lines of s points, points must fit in the line perfectly. Therefore, if a point ${}^{i,j}\boldsymbol{q}=({}^{i,j}u,\ {}^{i,j}v)$ fits in the straight line l, the following expression is true:

$$J_{ST} = \sum_{l=1}^{r}\sum_{i=1}^{s}\left(\boldsymbol{a_l}\,{}^{i,j}u + \boldsymbol{b_l}\,{}^{i,j}v + \boldsymbol{c_l}\right)^2 \tag{6}$$

where $\boldsymbol{a_l}$, $\boldsymbol{b_l}$, $\boldsymbol{c_l}$ represent the set of parameters which defines the straight line l. These parameters are computed with the s points belonging to the line. Again, vertical and horizontal straight lines must be taken into account. In Sections 2.1 and 2.2 of [34] a detailed description of how cross-ratio and straight line restrictions arise is done.

Joining both geometrical constraints J_{CR} and J_{ST} together with the pin-hole restrictions J_{PH}, the following functional arise:

$$\begin{aligned} J &= \sum_{j=1}^{m}\sum_{i=1}^{n}\left({}^{i,j}q - g(\boldsymbol{A},\boldsymbol{R}_j,\boldsymbol{t}_j,{}^{i}\boldsymbol{p})\right)^2 + \sum_{l} \\ &= 1^r \sum_{k=1}^{s-3}\left(CR(q^k,q^{k+1,l},q^{k+2,l},q^{k+3,l}) \right. \\ &\quad \left. - CR(\boldsymbol{p_1},\boldsymbol{p_2},\boldsymbol{p_3},\boldsymbol{p_4})\right)^2 + \sum_{l=1}^{r}\sum_{i=1}^{s}\left(\boldsymbol{a_l}\,{}^{i,j}u + \boldsymbol{b_l}\,{}^{i,j}v + \boldsymbol{c_l}\right)^2 \end{aligned} \tag{7}$$

To demonstrate that the optimization process is not under constrained, number of residuals must be greater than $2nm+5+6m$. To define the number of restrictions given with cross-ratio and straight lines restrictions, a squared chessboard is going to be considered where number of columns is equal to number of rows. This means that r is equal to s. If the number of points in the template is n, we have than $r=s=\sqrt{n}$. If m is the number of images and each image has horizontal and vertical lines, straight lines restriction gives $2m\cdot\sqrt{n}$ residuals. Referring to cross-ratio restriction, we have $s-3$ residuals with each set of points belonging to the same line. That means $\sqrt{n}-3$ residuals per line and $2(\sqrt{n}-3)$ per image taking into account that we have vertical and horizontal lines. Assuming m images, cross ratios restriction give $2m(\sqrt{n}-3)$ residuals. Using all residuals, expression (8) is always true and the optimization problem is over constrained. If $r>s$ or $r<s$ expression (8) remains

$$2mn+5+6m < 2mn+2m\sqrt{n}+2m(\sqrt{n}-3) \tag{8}$$

Initially we have thought about weighting each term of Eq. (7). Experimental results have show us that distorted control points ${}^{i,j}\boldsymbol{q_d}$ always converges to ${}^{i,j}\boldsymbol{q_p}$ which satisfy all template restrictions perfectly with independency of weight of terms J_{CR} and J_{ST} in Eq. (7). It is also seen that computed pin-hole model does not depend on the weight of J_{PH}. The result of the non-linear searching is a set of points which fit in the computed pin-hole model perfectly.

From the point of view of the number of images m used to obtain $\boldsymbol{A_p}$, $\boldsymbol{R_{pj}}$ and $\boldsymbol{t_{pj}}$, if $m\geq 3$ we will have a unique solution for the linear step, and the non-linear searching will converge to a place where undistorted control points of all images ${}^{i,j}\boldsymbol{q_p}$ satisfy all template restrictions perfectly. If the number of images increase the searching time increase also, but the result is always a set of control points of all images ${}^{i,j}\boldsymbol{q_p}$ satisfying template restrictions and an accurate camera model represented with $\boldsymbol{A_p}$, $\boldsymbol{R_{pj}}$ and $\boldsymbol{t_{pj}}$. If a template with 20 columns and 14 rows is used we have $20\times 14\times 2=560$ unknowns per image. With 10 images, unknowns will be as large as 5600 plus the pin-hole parameters. In our experiments, the non-linear searching has always converged to a place where points in images ${}^{i,j}\boldsymbol{q_p}$ satisfy all template restrictions perfectly, but the computing time has lasted from 1 min to 1 h. Since the camera calibration is an off-line process, it can be solved without problems.

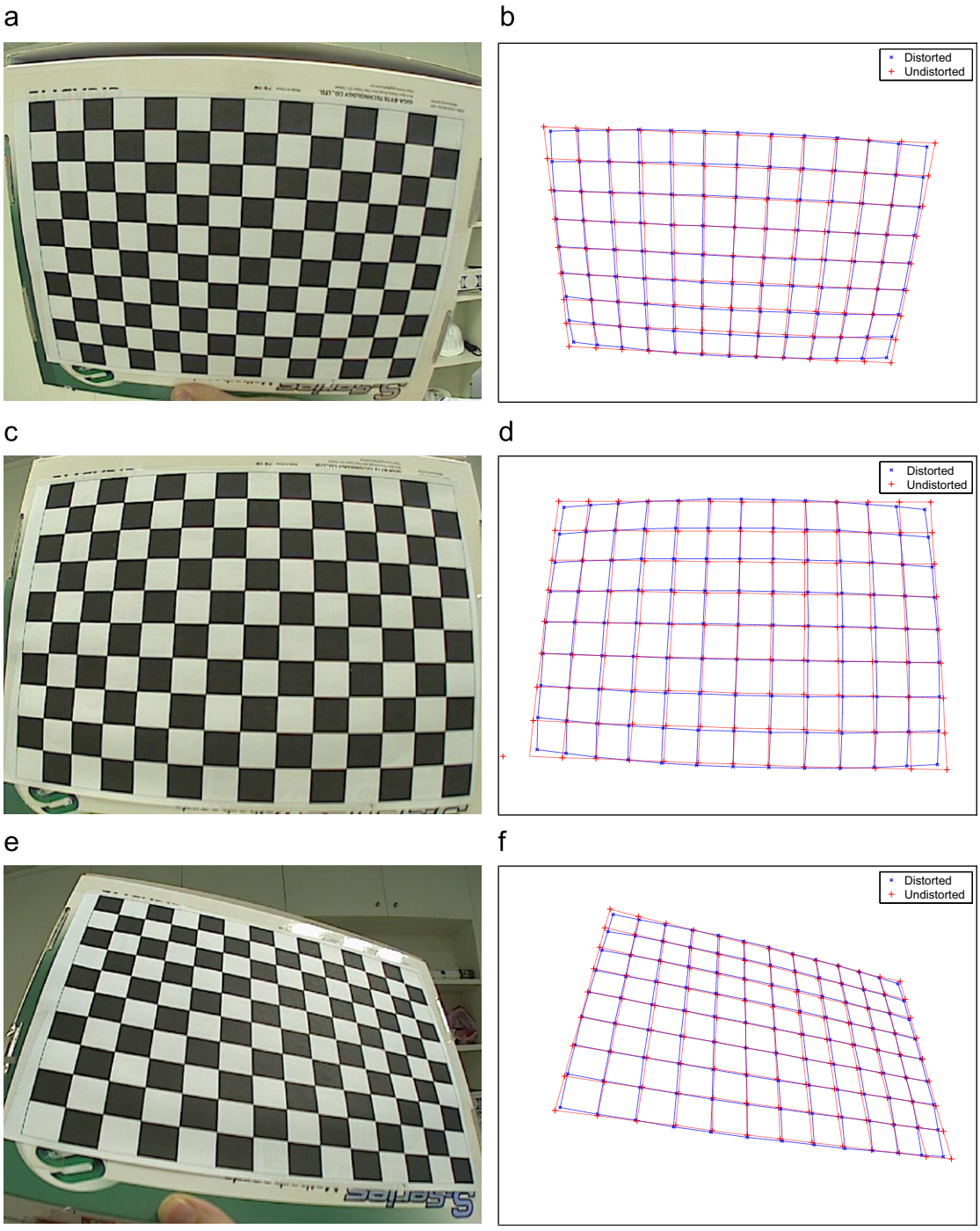

Fig. 1. (a)(c)(e) Image of the chessboard taken with an ethernet camera Axis 211 W with 8 mm lens mounted. (b)(d)(f) Detected points in the distorted image and corrected points positions according to the cross-ratio invariability, straight line restrictions and pin-hole model. Lens distortion is calibrated mapping the distorted point positions to their true positions.

If $m < 3$ calibration process can be solved also assuming some values to resolve the linear step as is shown in [24]. These assumptions are for example that the coordinates of the image principal point is located at the center of the CCD or that scale factors are equal in both image axes. If image is soft distorted, these assumptions can be true. However, hard distortions produces deviations of the principal point and changes in scale factors. These erroneous assumptions of the pin-hole model values give erroneous starting values to the non-linear searching. Therefore, when $m < 3$ the result of the non-linear searching can compute a pin-hole model $\boldsymbol{A_p}$, $\boldsymbol{R_{pj}}$ and $\boldsymbol{t_{pj}}$ which diverges to a place far away of the right one, although undistorted points ${}^{i,j}\boldsymbol{q_p}$ satisfy all template restrictions perfectly as before. The effect of the number of images in the calibration of the pin-hole model is tested in Section 4.

3.2. Adjusting lens distortion model

In the previous section, the method for correcting distorted control points in the image ${}^{i,j}\boldsymbol{q_d}$ and finding their true positions ${}^{i,j}\boldsymbol{q_p}$ has been described. Next steps consist of computing the parameters of the lens distortion model which maps from

distorted points ${}^{i,j}\boldsymbol{q_d}$ to undistorted points ${}^{i,j}\boldsymbol{q_p}$. For the proposed method, the number of images to resolve the model which maps from ${}^{i,j}\boldsymbol{q_d}$ to ${}^{i,j}\boldsymbol{q_{i,p}}$ is only one, although several images are necessary for the previous step and they can be used now. Since radial, decentering and prism distortion model does not represent high distortion lenses accurately; polynomial fish-eye distortion model described in Section 2 is calibrated here. Basu and Licardie [4] proposed using straight line restriction for adjusting the model. We propose a different method, since model is going to be adjusted to ${}^{i,j}\boldsymbol{q_d}$ and ${}^{i,j}\boldsymbol{q_{i,p}}$. In this case, using a set of nm points ${}^{i,j}\boldsymbol{q_d}$, ${}^{i,j}\boldsymbol{q_{i,p}}$ per image give nm pairs $(r_{i,d}, r_{i,0})$. The objective of the least squares method is to minimize the following error function:

$$J_{PFET} = \sum_{i=1}^{nm} \left(r_{i,d} - \sum_{t=0}^{ka} (a_t r_{i,O}^T) \right)^2 \tag{9}$$

where k_a represents the degree of the polynomial fish-eye distortion model. In this case fifth order has been considered for k_a. The degree of the polynomial fish-eye distortion model is not significant to the computation process. To minimize this set of linear equations, the Levenberg–Marquart algorithm has been used. Distortion center is initialized with the principal point and initial values for $a_{1,\ldots,5}$ are obtained with a closed form solution using the nm pairs $(r_{i,d}, r_{i,p})$ for $a_{0,\ldots,5}$. For $a_{0,\ldots,5}$ following expression arise:

$$\begin{bmatrix} 1 & r_{1,p} & r_{1,p}^2 & r_{1,p}^3 & r_{1,p}^4 & r_{1,p}^5 \\ \ldots & \ldots & \ldots & \ldots & \ldots & \ldots \\ 1 & r_{nm,p} & r_{nm,p}^2 & r_{nm,p}^3 & r_{nm,p}^4 & r_{nm,p}^5 \end{bmatrix} \cdot \begin{bmatrix} a_0 \\ a_1 \\ a_2 \\ a_3 \\ a_4 \\ a_5 \end{bmatrix} = \begin{bmatrix} r_{1,d} \\ \ldots \\ r_{nm,p} \end{bmatrix} \tag{10}$$

If (10) is expressed as $\boldsymbol{W}\cdot\boldsymbol{x}=\boldsymbol{w}$, where $x=[a_0, a_1, a_2, a_3, a_4, a_5]^T$, the linear least square solution is given by $\boldsymbol{x}=(\boldsymbol{W}\cdot\boldsymbol{W})^{\boldsymbol{T}}\cdot\boldsymbol{W}^{\boldsymbol{T}}\cdot\boldsymbol{w}$.

4. Experimental results

The proposed calibration technique is compared with existing calibration methods. One method was proposed by Zhang [24] and is freely available. This method carries out a full camera calibration method (FCCM), which computes external (rotation and translation) and internal camera parameters at the same time. The internal parameters are the pin-hole camera parameters and also the second order radial distortion parameters. The center of the radial distortion is considered as the principal point. A closed-form solution is first solved to obtain the starting values of the non-linear search.

The second method is a non-metric calibration method (NMLDC). It consists of computing the lens distortion and the pin-hole model separately. First the polynomial lens distortion model is calibrated using the technique proposed by Basu and Licardie [4]. In this case, the non-linear optimization step may lead to instability if the distortion center and distortion coefficients are computed together with a few points [4]. With the computed polynomial distortion model, detected points in the image are corrected and the pin-hole model is calibrated using undistorted points. The pin-hole model is computed using the FCCM but without calibrating lens distortion.

Finally the lens distortion and pin-hole models are adjusted using the metric method (MLDC) proposed in this paper. First pin-hole model is adjusted and detected points in the image are corrected. Second the polynomial lens distortion model is adjusted with distorted and corrected set of points. Methods are tested on computer simulated data and real data.

For measuring the calibration error, the normalized calibration error (NCE) proposed by [22] is used. The NCE is calculated as follows:

$$e_n = \frac{1}{n}\sum_{i=1}^{n} \sqrt{\frac{({}^*x_i - x_i)^2 + ({}^*y_i - y_i)^2}{z_i\left(\alpha^{-2}+\beta^{-2}\right)/12}} \tag{11}$$

where ${}^*\boldsymbol{p_i}=({}^*x_i, {}^*y_i, z_i)$ represents 3D camera coordinates as estimated by back-projection form 2D undistorted pixel coordinates to depth z_i and $\boldsymbol{p_i}=(x_i, y_i, z_i)$ represents observed 3D camera coordinates computed from measured 3D world coordinates. The values of α and β can be calculated using the intrinsic camera parameters. If $NCE \approx 1$, this indicates calibration is good and residual distortion is negligible compared with image digitization noise at this depth. NCE $\gg 1$ reveals poor calibration and $NCE \ll 1$ corresponds to a calibration whose error is lower, on average, than the digitization noise of a pixel at this depth. The depth z_i of the point to the image plane is computed depending on whether simulated or real data are used. With simulated data, the depth of each point to the image plane is known, since the calibration scene is simulated and the precise camera parameters are known. In the case of real data, the camera must be calibrated to obtain the back-projection of the undistorted pixel coordinates.

4.1. Computer simulations

The simulated camera has an image scale factor $s_x=1.5$ and an effective focal length $f=8$, resulting in pixel focal lengths of $\alpha=750$ and $\beta=750$. The image resolution is 640×480 and with the principal point of the image at (320,240) pixels. The skew factor is set to $\gamma=0$.

The training model plane is a 210 mm $\times$ 297 mm checkerboard with 280 corners points (14×20), similar to that shown in Fig. 1. The images are taken from 20 different orientations in front of the virtual camera. Images of the checkerboard are taken according to the pin-hole model and are distorted using the non-linear polynomial distortion model. Two levels of distortion are applied simulating low and high distortion. For high distortion a third-order radial distortion is simulated with the coefficients $k_1=-0.3\ \text{mm}^{-2}$, $k_2=-0.045\ \text{mm}^{-2}$. Second order tangential distortion is added with $p_1=-0.005\ \text{mm}^{-2}$ and $p_2=-0.00025\ \text{mm}^{-2}$. Prism distortion is discarded and the distortion center is simulated at $u_0=305$ and $v_0=257$ pixels. Low distortion is simulated with $k_1=-0.2\ \text{mm}^{-2}$, $k_2=0$, $p_1=p_2=0$ and $u_0=317$, $v_0=244$ pixels. 15 images are used to compute the parameters and 5 to test the results. Gaussian noise of mean 0 and standard deviation σ is added to the point's coordinates of the images. σ is added to the image in front of the camera when the model plane is parallel with the image plane and depending on the angle between model and the image plane, σ is increased to 2σ with 70°. This simulates the influence of the point's detection in the image, depending on the angle between the image plane and the model plane. No noise is added to test data.

Calibration accuracy vs. pixel coordinates noise: Figs. 2 and 3 show the decrease of accuracy (normalized calibration error) if pixel noise in training and test data increases. Fig. 2 shows the simulation results of low lens distortion and Fig. 3 shows those for high lens distortion. NMLDC is more sensitive to pixel noise. This is because lens distortion and pin-hole models are computed separately and errors cannot be compensated. With FCCM, calibration errors with distortion parameters are compensated with the camera pin-hole parameters. However, this compensation is only true for the calibration step since lens distortion and camera parameters satisfy the set of training data. When data change, the computed model no longer satisfies them. Similar

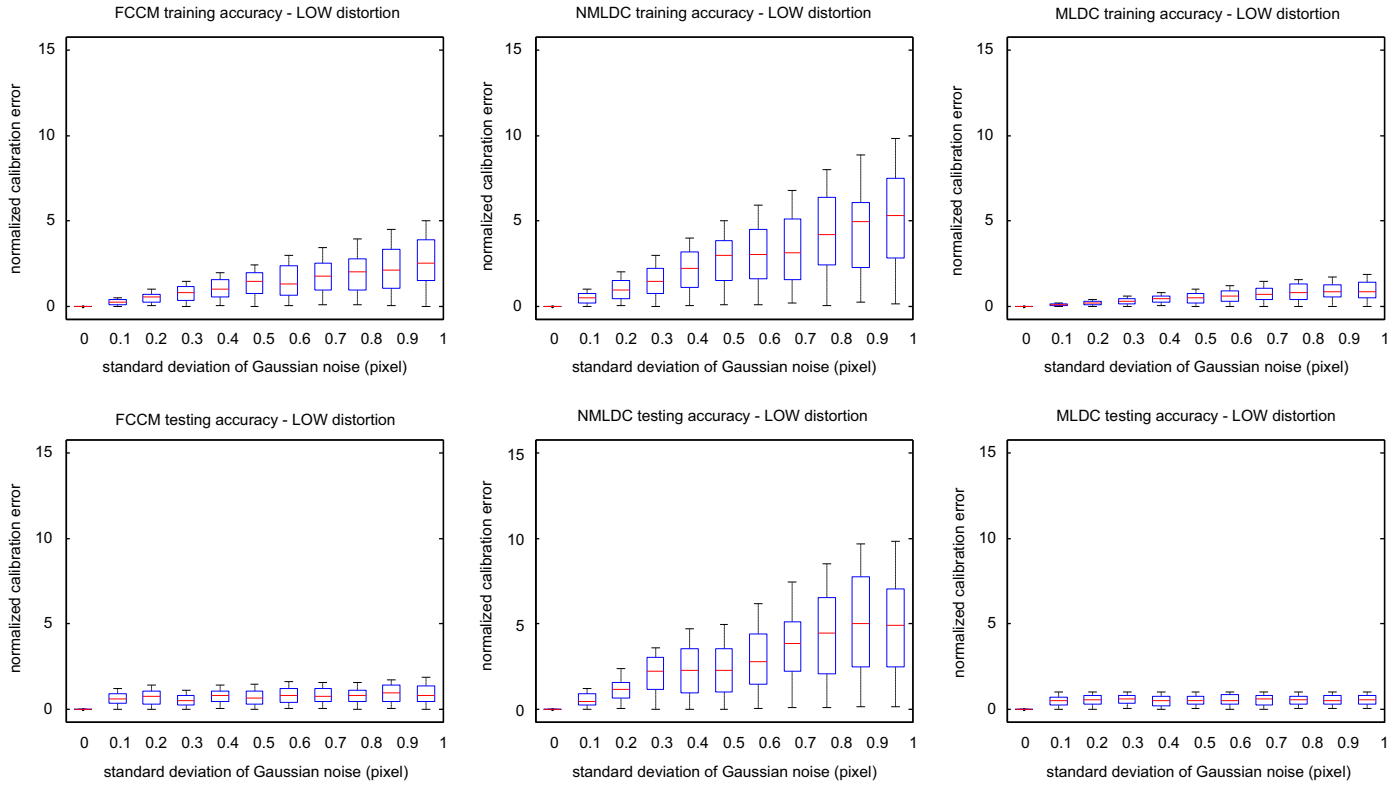

Fig. 2. Effects of pixel coordinate noise on calibration accuracy. Gaussian noise is added to training data but not to testing data. Low lens distortion is simulated.

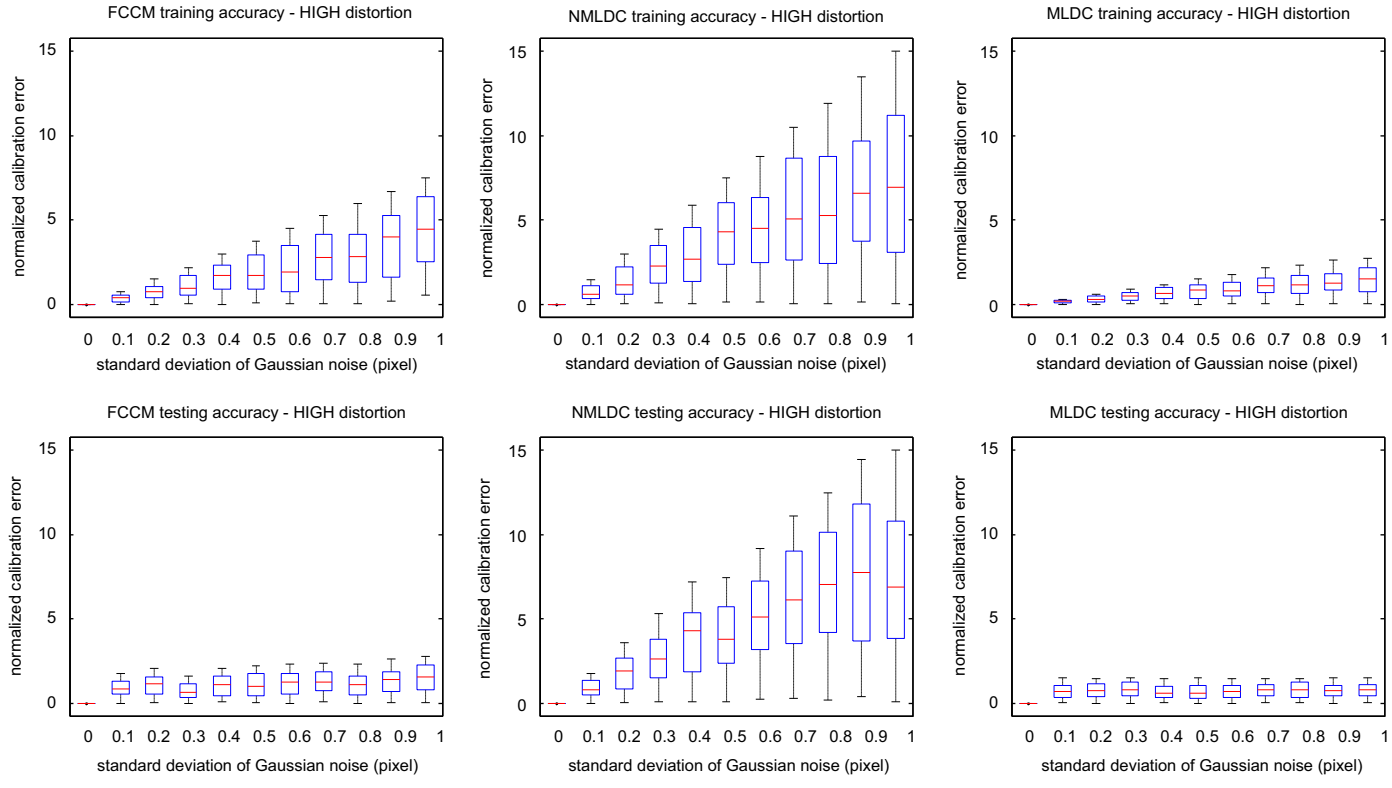

Fig. 3. Effects of pixel coordinates noise on calibration accuracy. Gaussian noise is added to training data but not to testing data. High lens distortion is simulated.

results were obtained by Sun and Cooperstock [33]. Finally with MLDC, lens distortion is represented by the computed model and when the data change the normalized error is similar. In this case, calibration of the camera pin-hole model is independent of calibration of lens distortion and does not depend on the training data.

Calibration accuracy vs. number of points: Figs. 4 and 5 show the effect of the number of data in the calibration process. In the absence of noise, a small number of training points can yield 100% accuracy. Some existing corner detection algorithms claim an accuracy of 0.1 pixels, Gaussian noise of zero mean and $\sigma=0.1$ is added to the pixel coordinates of the training data. The average of the results of 25 trials is shown in Figs. 4 and 5. Again NMLDC gives greater errors.

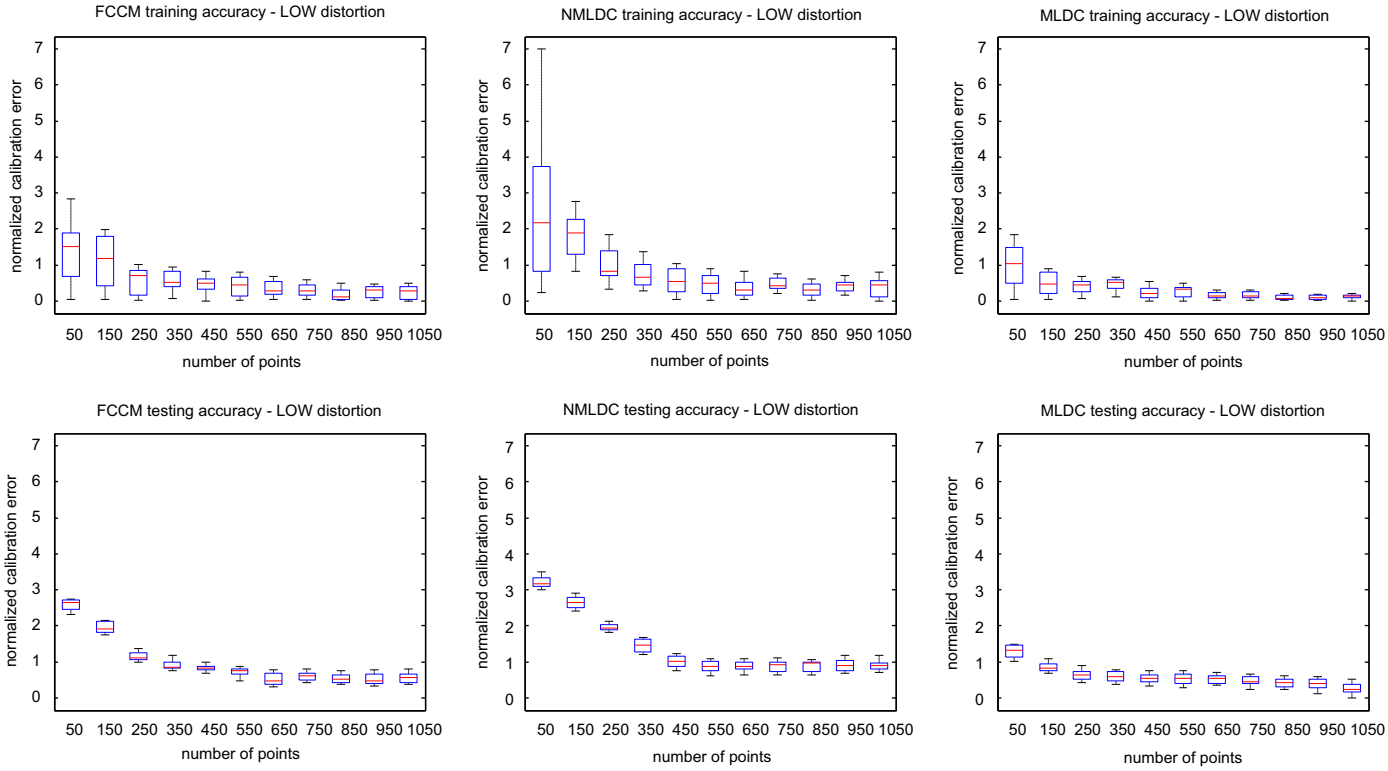

Fig. 4. Effects of training data quantity on calibration accuracy. Gaussian noise of $\sigma=0.1$ is added to training data but not to testing data. Low lens distortion is simulated.

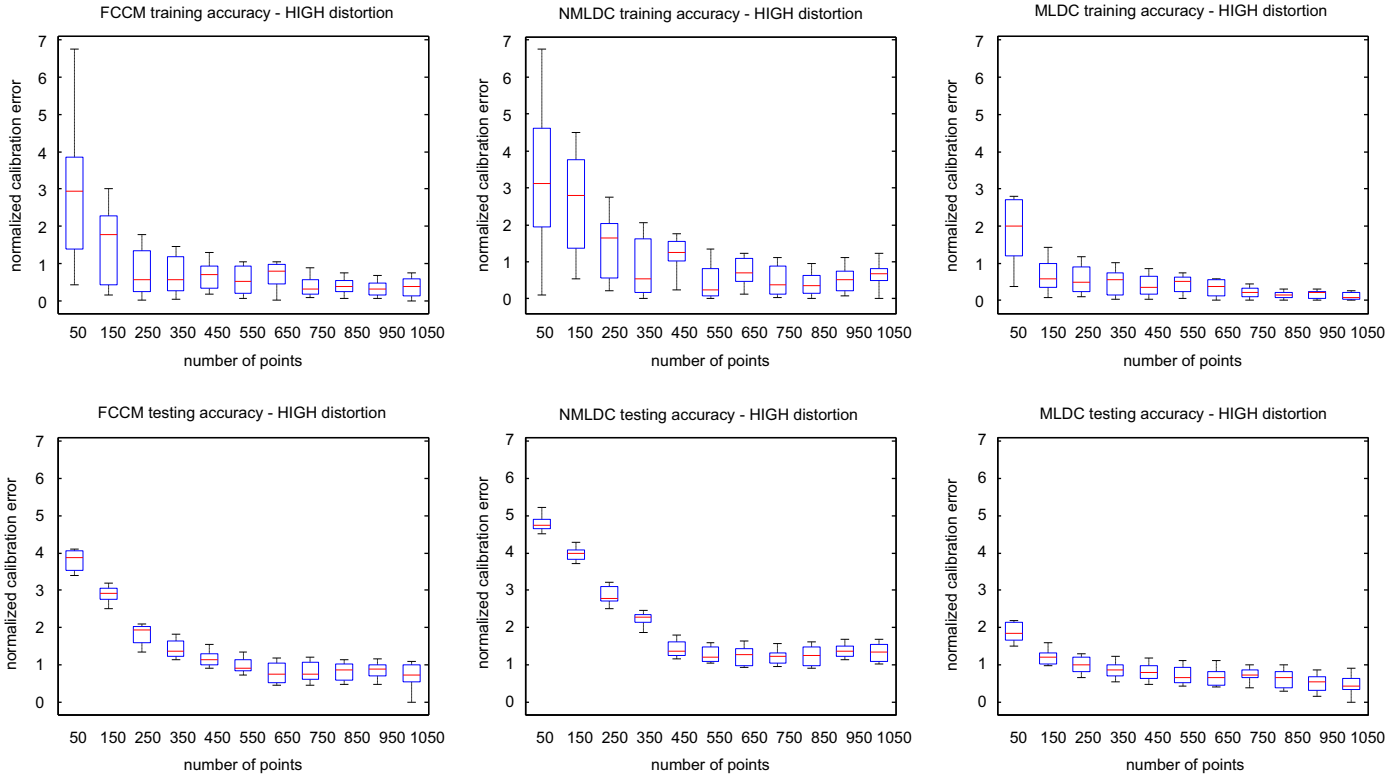

Fig. 5. Effects of training data quantity on calibration accuracy. Gaussian noise of $\sigma=0.1$ is added to training data but not to testing data. High lens distortion is simulated.

4.2. Real data

We have used a low-cost Ethernet camera Axis 211 W with 8 mm lens mounted. The image acquired was of 640×480 pixels with considerable distortion. Fig. 1a, c and e shows several images from Axis 211 W used to calibrate the camera. The optimization step was performed using the "lsqnonlin" subroutine from Matlab. Corner detection was made with the function cvFindChessboardCorners() from openCV library. The training data was generated by printing a chessboard pattern of 15×11 grid corners onto letter-size sheets and viewed at 20 different orientations at roughly 45° with respect to the camera plane. This produced 20 data sets of 165 points. Fifteen were used to compute the parameters and five to test the results. In this case, calibration method and distortion model were compared.

Calibration technique accuracy vs. number of points: Fig. 6 shows the effect in the calibration process when the number of points changes. In this case, one calibration is performed with each set of points and normalized error is shown in Fig. 6. Results are quite similar to the simulation step. The FCCM method obtains low normalized calibration error if training data is used. If testing data is used, the normalized calibration error increases. This is because with FCCM, parameters are adjusted to satisfy the set of training data and do not represent the lens distortion model and camera model really. When pin-hole camera parameters are computed separately from lens distortion parameters, they adjust testing and training data if MLDC is used. The NMLDC method computes models which fit in training data but does not represent camera performance accurately. Fig. 6 shows this effect. Undistorted images with each method are shown in Fig. 7. Distortion correction with MLDC method seems to be more accurate than undistorted images with the NMLDC or FCCM methods.

Calibration technique: Pin-hole model computed with each calibration methods has been compared. The computed parameters are shown in Table 1. The FCCM method obtains better results in the training step. This is because lens distortion calibration errors are compensated with the camera pin-hole parameters. If lens distortion model is calibrated separately of the camera pin-hole model, training errors are similar to the testing errors if the MLDC is used. This result is similar to results with simulated data.

5. Conclusions

A new calibration method is proposed with better performance than existing calibration methods. To date, camera calibration is resolved computing lens distortion together with camera parameters or computing the lens distortion in isolation from the pin-hole model. If lens distortion is computed alone then instabilities occur. If lens distortion is computed together with camera parameters, both sets of parameters satisfy the training data since errors are mutually compensated. However, if data changes then the computed models do not work as well as in the calibration step. To resolve the calibration instabilities and the model coupling, a method is proposed to compute the lens distortion in isolation from the pin-hole model. Using several images of a planar template, images are undistorted to match those in a pin-hole model. In the second step, using detected distorted points and the computed undistorted points, a metric process is used to calibrate the distortion model. This method guaranties stability when non-linear searching is solved and also when the distortion center is computed. The model decouples the pin-hole and lens distortion models since they are computed separately.

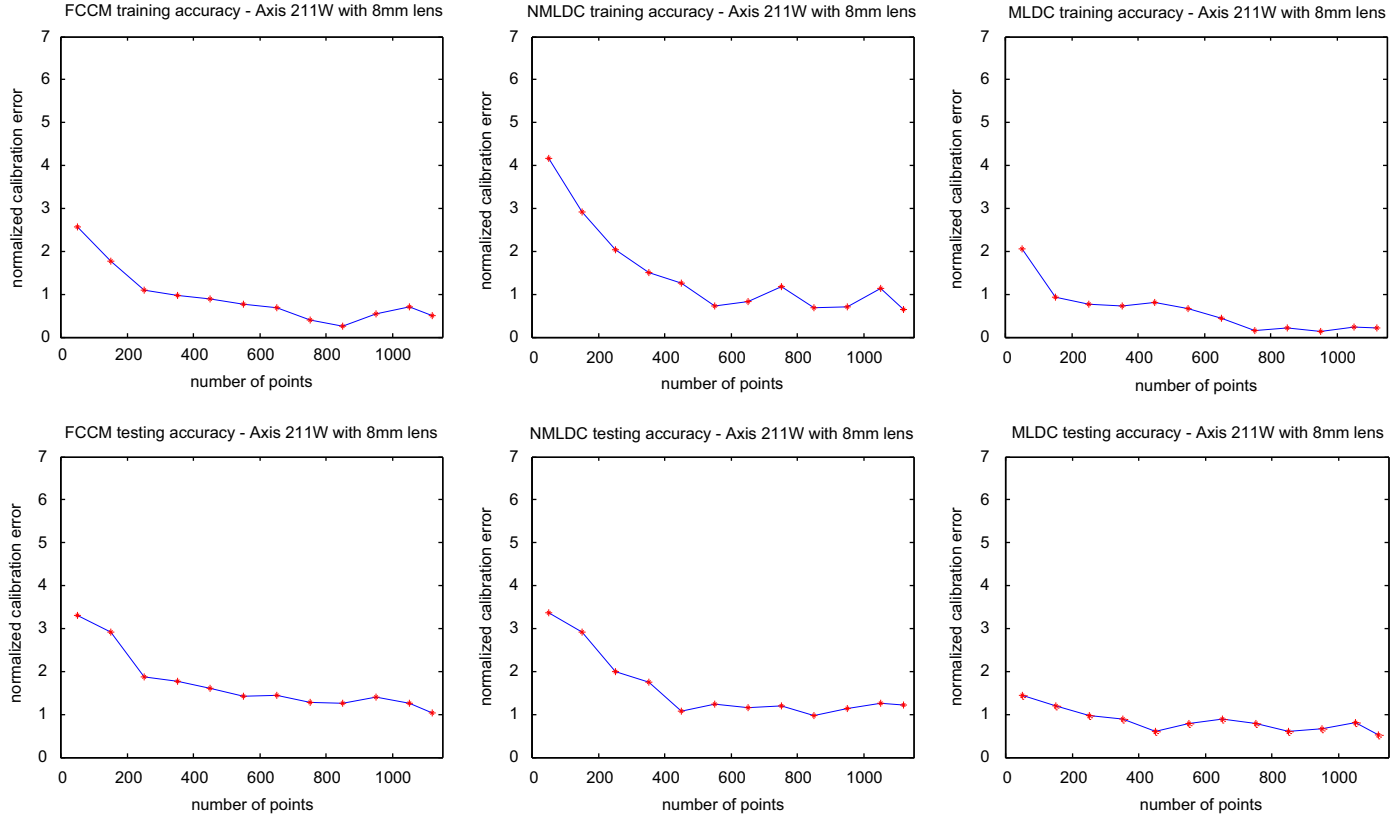

Fig. 6. Effects of training data quantity on calibration accuracy with a real ethernet camera Axis 211 W with 8 mm lens.

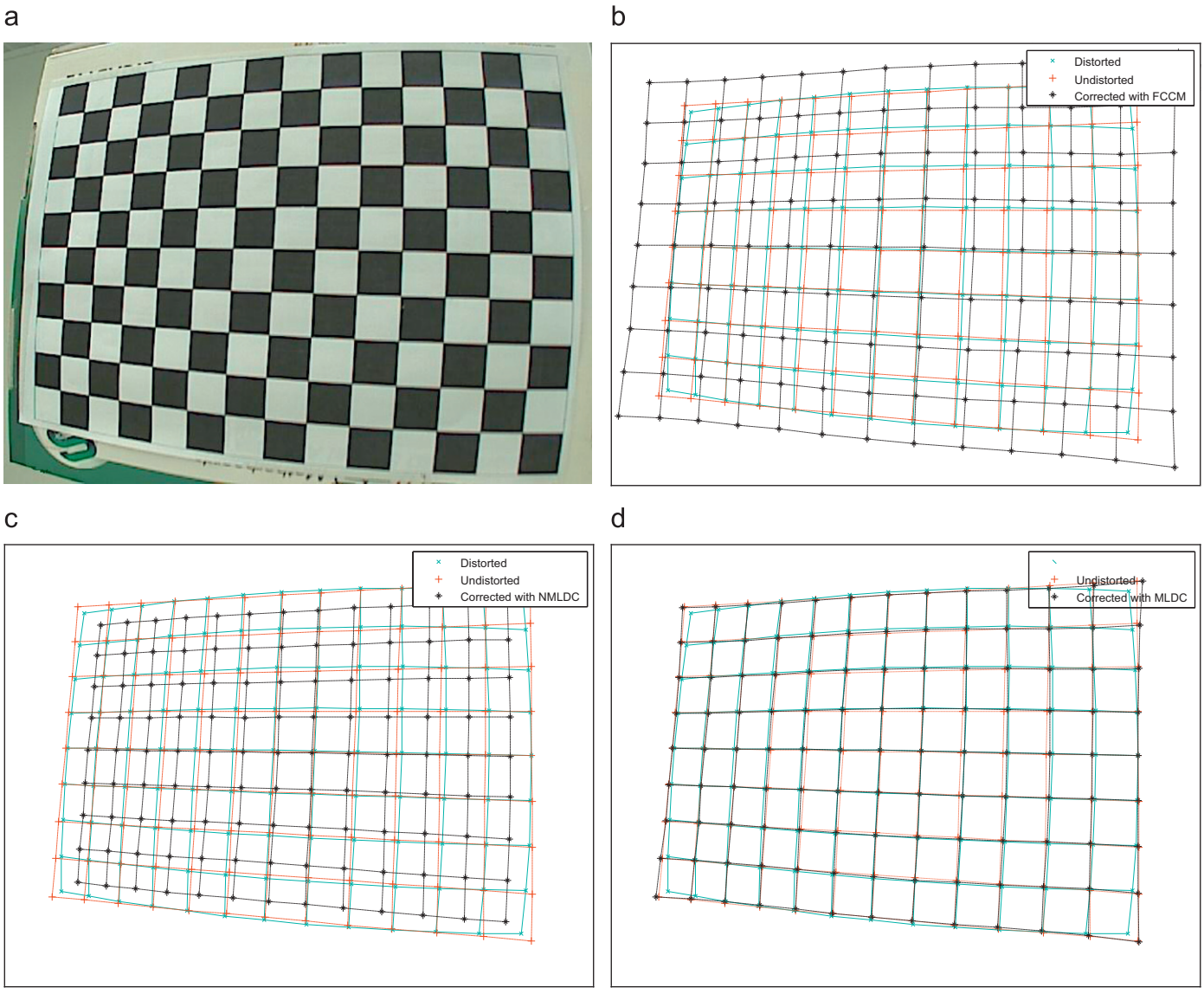

Fig. 7. (a) Image of the chessboard taken with the Ethernet camera Axis 211 W with 8 mm lens. (b) Image corrected with the distortion model computed together with the pin-hole model using Zhang's calibration technique [24] based on a 2D template. (c) Image corrected with the distortion model computed alone using the calibration technique of Basu and Licardie [4], which is based on the idea that straight lines in the image have to be straight. (d) Image corrected with the distortion model computed using the pin-hole method presented in this paper. Similarities between the original and the undistorted image increase if the calibration technique presented in this paper is used (squares corners are closer).

Table 1
Pin-hole parameters computed with different methods.

		FCCM	NMLDC	MLDC
Pin-hole model	fx	547.84	592.07	606.37
	fy	503.89	535.78	555.47
	c_u (pixels)	293.36	308.45	282.80
	c_v (pixels)	235.62	229.07	241.70
	γ (deg)	87.46	89.77	90
Training error		**1.496**	**2.071**	**1.547**
Testing error		**3.651**	**2.924**	**1.784**

Acknowledgments

This work was partially funded by the Universidad Politécnica de Valencia research funds (PAID 2010, Project no. 2431) and by Spanish government and the European Community under the project nos. DPI2010-20814-C02-02 (FEDER-CICYT) and DPI2010-20286 (CICYT).

References

[1] Wang J, Shi F, Zhang J, Liu Y. A new calibration model of camera lens distortion. Pattern Recognition 2008;41:607–15.
[2] Brown DC. Decentering distortion of lenses. Photogrammetric Engineering and Remote Sensing 1966;24:555–66.
[3] Brown DC. Close-range camera calibration. Photogrammetric Engineering and Remote Sensing 1971;42:855–66.
[4] Basu A, Licardie S. Alternative models for fish-eye lenses. Pattern Recognition Letters 1995;16:433–41.
[5] Beauchemin SS, Bajcsy R. Modelling and removing radial and tangential distortions in spherical lenses, multi image analysis. Lecture Notes in Computer Science 2001;2023:1–21.
[6] McGlone C, Mikhail E, Bethel J, editors. 5th ed. American Society of Photogrammetry and Remote Sensing; 2004.
[7] Ma L, Chen YQ, Moore KL. Flexible camera calibration using a new analytical radial undistortion formula with application to mobile robot localization. In: IEEE international symposium on intelligent control, 2003.
[8] Mallon J, Whelan PF. Precise radial un-distortion of images. In: Proceedings of the 17th international conference on pattern recognition, 2004.
[9] Shah S, Aggarwal JK. Intrinsic parameter calibration procedure for a (high distortion) fish-eye lens camera with distortion model and accuracy estimation. Pattern Recognition 1996;29:1775–8.
[10] Sturm P, Ramalingam S. A generic concept for camera calibration. In: Proceedings of the fifth European conference on computer vision, 2004.

[11] Devernay F, Faugeras O. Straight lines have to be straight. Machine Vision Applications 2001;13:14–24.
[12] Fitzgibbon A. Simultaneous linear estimation of multiple view geometry and lens distortion. In: IEEE international conference on computer vision and pattern recognition, 2001.
[13] Prescott B, McLean G. Line-based correction of radial lens distortion. Graphical Models and Image Processing 1997;59:39–47.
[14] Swaminathan R, Nayar S. Non metric calibration of wide-angle lenses and polycameras. IEEE Transactions on Pattern Analysis and Machine Intelligence 2002;22:1172–8.
[15] Ahmed M, Farag A. Non-metric calibration of camera lens distortion: differential methods and robust estimation. IEEE Transactions on Image Processing 2005;14:1215–30.
[16] Becker S, Bove V. Semi-automatic 3D model extraction from uncalibrated 2D camera views. Proceedings of Visual Data Exploration and Analysis II 1995;2:447–61.
[17] Zhang G, He J, Yang X. Calibrating camera radial distortion with cross-ratio invariability. Optics and Laser Technology. 2003;35:457–61.
[18] Penna M. Camera calibration: a quick and easy way to detection of scale factor. IEEE Transactions on Pattern Analysis and Machine Intelligence 1991;12:1240–5.
[19] Zhang Z. On the epipolar geometry between two images with lens distortion. Proceedings of the International Conference on Computer Vision and Pattern Recognition 1996;1:407–11.
[20] Stein G. Lens distortion calibration using point correspondences. In: Proceedings of the international conference on computer vision and pattern recognition, 1997.
[21] Tsai R. A versatile camera calibration technique for high-accuracy 3D machine vision metrology using off-the-self TV camera lenses. IEEE Journal of Robotics and Automation 1987;RA-3:323–44.
[22] Weng J, Cohen P, Herniou M. Camera calibration with distortion models and accuracy evaluation. IEEE Transactions on Pattern Analysis and Machine Intelligence 1992;14:965–80.
[23] Wei J, Ma S. Implicit and explicit camera calibration: theory and experiments. IEEE Transactions on Pattern Analysis and Machine Intelligence 1994;16: 15–20.
[24] Zhang Z. A flexible new technique for camera calibration. IEEE Transactions on Pattern Analysis and Machine Intelligence 2000;22:1330–4.
[25] Zhang Z. Camera calibration with one-dimensional objects. IEEE Transactions on Pattern Analysis and Machine Intelligence 2004;26:892–9.
[26] He BW, Li YF. Camera calibration from vanishing points in a vision system. Optics and Laser Technology 2008;40:555–61.
[27] Song LM, Wang MP, Lu L, Huan HJ. High precision camera calibration in vision measurement. Optics and Laser Technology 2007;39:1413–20.
[28] Hartley R, Kang S. Parameter-free radial distortion correction with centre of distortion estimation. In: Proceedings of the 10th international conference on computer vision, 2005.
[29] Lavest J, Viala M, Dhome M. Do we really need accurate calibration pattern to achieve a reliable camera calibration. European Conference on Computer Vision 1998;1:158–74.
[30] Bräuer-Burchardt C, Voss K. A new algorithm to correct fish-eye- and strong wide-angle-lens-distortion from single images. In: Proceedings of the IEEE international conference on image processing, 2001.
[31] Schneider D, Schwalbe E, Maas H-G. Validation of geometric models for fisheye lenses. ISPRS Journal of Photogrammetry Remote Sensing 2009;64: 259–66.
[32] Hughes C, Denny P, Jones E, Glavin M. Accuracy of fish-eye lens models. Applied Optics 2010;49:3338–48.
[33] Sun W, Cooperstock JR. An empirical evaluation of factors influencing camera calibration accuracy using three publicly available techniques. Machine Vision and Applications 2006;17:51–67.
[34] Ricolfe-Viala C, Sanchez-Salmeron AJ. Correcting non-linear lens distortion in cameras without using a model. Optics and Laser Technology 2010;42:628–39.